This is an open access article published under an ACS AuthorChoice License, which permits copying and redistribution of the article or any adaptations for non-commercial purposes.

ARTICLE

Van der Waals Epitaxy of Two-Dimensional MoS_2−Graphene Heterostructures in Ultrahigh Vacuum

Jill A. Miwa, Maciej Dendzik, Signe S. Grønborg, Marco Bianchi, Jeppe V. Lauritsen, Philip Hofmann, and Søren Ulstrup*,†

Department of Physics and Astronomy, Interdisciplinary Nanoscience Center, Aarhus University, 8000 Aarhus C, Denmark. †Present address: Advanced Light Source, E.O. Lawrence Berkeley National Laboratory, Berkeley, California 94720, USA.

ABSTRACT In this work, we demonstrate direct van der Waals epitaxy of MoS_2−graphene heterostructures on a semiconducting silicon carbide (SiC) substrate under ultrahigh vacuum conditions. Angle-resolved photoemission spectroscopy (ARPES) measurements show that the electronic structure of free-standing single-layer (SL) MoS_2 is retained in these heterostructures due to the weak van der Waals interaction between adjacent materials. The MoS_2 synthesis is based on a reactive physical vapor deposition technique involving Mo evaporation and sulfurization in a H_2S atmosphere on a template consisting of epitaxially grown graphene on SiC. Using scanning tunneling microscopy, we study the seeding of Mo on this substrate and the evolution from nanoscale MoS_2 islands to SL and bilayer (BL) MoS_2 sheets during H_2S exposure. Our ARPES measurements of SL and BL MoS_2 on graphene reveal the coexistence of the Dirac states of graphene and the expected valence band of MoS_2 with the band maximum shifted to the corner of the Brillouin zone at $\bar{K}$ in the SL limit. We confirm the 2D character of these electronic states *via* a lack of dispersion with photon energy. The growth of epitaxial MoS_2−graphene heterostructures on SiC opens new opportunities for further *in situ* studies of the fundamental properties of these complex materials, as well as perspectives for implementing them in various device schemes to exploit their many promising electronic and optical properties.

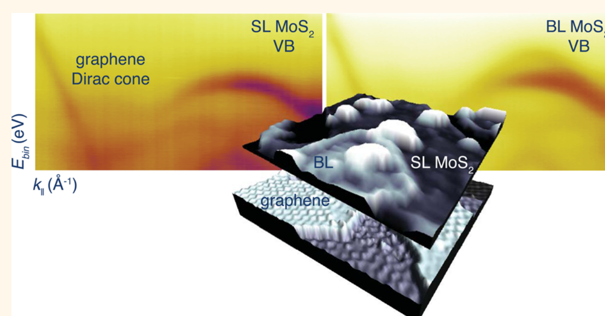

KEYWORDS: 2D material heterostructures · graphene · transition metal dichalcogenides · MoS_2 · van der Waals epitaxy · angle-resolved photoemission spectroscopy · scanning tunneling microscopy

Interesting new physics and opportunities for designing novel electronic devices emerge when stacking two-dimensional (2D) crystals in so-called van der Waals heterostructures.[1] Apart from the possibility of protecting reactive 2D materials with the rather inert graphene, such structured materials offer the intriguing possibility, for example, to combine the relativistic Dirac particles that exist in graphene[2] with the strongly bound excitons that can be generated in the transition metal dichalcogenides (TMDCs).[3,4] Many TMDCs constitute a class of 2D direct gap semiconductors in the single layer (SL) limit where MoS_2 has been a forefront material in this research field—a development that can be attributed to the fact that SL MoS_2 is easily isolated from its bulk crystal counterpart by mechanical exfoliation.[5,6] This approach has unveiled a great variety of phenomena associated with the coupling of electron spin and valley degrees of freedom in the material, such as valley polarization in the photoluminescence from the primary exciton line.[7−9] Recent advances in synthesis methods have led to the realization of other SL TMDCs, such as $MoSe_2$ and WSe_2, revealing that many of the interesting traits in MoS_2 are also carried over to these materials.[10−14] Stacking SL TMDCs and graphene has led to vertical tunneling transistors with high on−off ratios and efficient optoelectronic devices—achievements which hinge on the combination of a direct band gap in SL TMDCs and excellent carrier transport behavior in graphene.[15−18] Combining the different SL TMDCs in heterostructures

* Address correspondence to sulstrup@lbl.gov.

Received for review April 19, 2015 and accepted June 3, 2015.

Published online June 03, 2015
10.1021/acsnano.5b02345

© 2015 American Chemical Society

conserves the direct band gap in each material, resulting in improved optical absorption and the possibility of engineering excitons by separating electron−hole pairs between the TMDC layers.[19−22]

Direct large-area growth of TMDC−graphene heterostructures is preferable for a large variety of *in situ* characterization techniques to extract material properties, and it is a basic requirement for realistic applications. These 2D heterostructures can be synthesized using van der Waals epitaxy. This approach relies on the relatively weak (van der Waals) coupling between the adjacent 2D materials and does not require that their crystal lattices match. This is in contrast to standard epitaxy methods. Graphene has proven to be a useful template in itself for such an approach, as exemplified by the successful growth of other low-dimensional systems on graphene such as III−V semiconductor nanowires[23] and thin films[24] as well as topological insulators.[25] MoS_2 and other TMDCs have been grown by chemical vapor deposition (CVD) methods using suitable carrier gases in furnace systems on either CVD graphene on copper,[26] sapphire,[27] or graphene transferred onto SiO_2.[28] Alternatively, high-quality epitaxial graphene on wide band gap silicon carbide (SiC) substrates has proven to be a good template for van der Waals epitaxy of MoS_2 and WSe_2 in CVD furnaces.[13,14] Growing these directly on such insulating substrates elegantly removes the need for additional transfer steps for further electrical or optical measurements.

A disadvantage of these CVD approaches is that the growth process cannot be studied *in situ*. In fact, moving samples from the CVD system through air could, in principle, lead to contamination and formation of defects. It is a key issue to control and understand the role of such defects, as these have been shown to play a pivotal role in electron transport[29] and ultrafast dynamics.[30−32] So far, *in situ* growth in ultra-high vacuum (UHV) of TMDC−graphene heterostructures has only been demonstrated for the material system $MoSe_2$/graphene/SiC using molecular beam epitaxy (MBE).[11,12]

In comparison to the synthesis methods mentioned above, we offer an alternative route that enables van der Waals epitaxy of sulfur-based TMDCs on graphene in UHV. Here we focus on SL MoS_2 due to future prospects of using surface-sensitive spectroscopic techniques to directly explore the intriguing spin and valley properties reported for this material.[7] The quartet of SL TMDCs (MoS_2, WS_2, $MoSe_2$, WSe_2) has thus come within reach for *in situ* characterization techniques.[11] We believe that this will facilitate studies with a new level of insight into the differences between these materials and how their properties are affected by underlying substrates or in various heterostructure combinations. Here, we take the opportunity to characterize the growth of MoS_2 on epitaxial graphene on SiC in detail using scanning tunneling microscopy (STM). High coverage SL and bilayer (BL) films of MoS_2 are achieved, which we exploit to determine their electronic structure on graphene using angle-resolved photoemission spectroscopy (ARPES).

RESULTS AND DISCUSSION

In order to synthesize MoS_2, we use a physical vapor deposition (PVD) method involving the evaporation of atomic Mo onto a substrate from a solid Mo source mounted in an electron beam evaporator. After Mo deposition, the substrate is annealed (≈1050 K), and since the entire process is carried out in a low-pressure H_2S atmosphere (≈1×10^{-5} mbar), it facilitates the reaction between Mo and S to form MoS_2. The growth is performed *in situ* in a UHV chamber with a base pressure in the low 10^{-10} mbar range. This general approach has already been proven successful for obtaining epitaxial SL MoS_2 on a Au(111) substrate.[33] An explanation for the high-quality nature of the grown films in these studies may be attributed to a sufficiently strong MoS_2−Au interaction that drives the epitaxial alignment of the MoS_2 with the substrate. This interaction is also confirmed by the discernible moiré pattern in the MoS_2 film. Transferring this approach to SL graphene on silicon carbide (G/SiC), which exhibits a much weaker van der Waals interaction with MoS_2, requires adjustments to the growth procedure that we discuss in the following.

The G/SiC substrate was synthesized in UHV by direct current annealing of SiC under a mild flux of Si atoms as described elsewhere[34,35] and in further details in the Materials and Methods section. The STM image in Figure 1a shows the clean G/SiC surface along with the characteristic SL graphene lattice, which can be atomically resolved at low bias (see inset). At higher bias, the underlying SiC strongly influences the way the graphene is imaged by the STM.[36,37] The quality and dominant layer thickness of the graphene is also checked using ARPES (not shown), where we observe a single, sharp, and electron-doped Dirac cone, as expected for samples without the presence of BL graphene.[38] The doping is caused by a buffer layer with a $(6\sqrt{3} \times 6\sqrt{3})R30°$ periodicity between graphene and SiC,[39] which we observe by STM to coexist with graphene regions in our samples. The presence of such buffer layer areas is a key element in the growth of MoS_2, which we follow in its initial stages in Figure 1b−f. The details of the growth are also outlined in the Materials and Methods section.

Evaporation of Mo is carried out using a Mo flux and duration that gives the submonolayer Mo coverage shown in the STM image in Figure 1b. Without H_2S, the Mo appears as small, bright, rounded clusters. The G/SiC substrate is held at room temperature during evaporation, which ensures a low Mo mobility, thereby

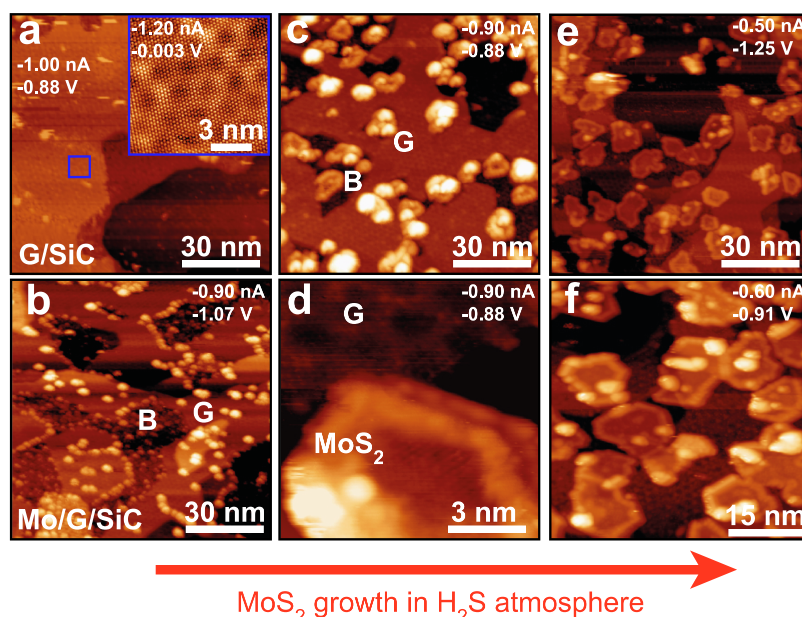

Figure 1. (a) STM image of the graphene/SiC (G/SiC) substrate. Inset: Atomic resolution image of the graphene lattice within the area marked by the blue square. (b) Sample surface after evaporation of atomic Mo (Mo/G/SiC). Buffer layer (B) and single-layer graphene (G) areas are distinguishable *via* the different distribution of adsorbed Mo. (c) MoS_2 nanoislands grown in B regions after annealing at 1050 K in a H_2S atmosphere. (d) Atomic resolution image of a 6 nm wide MoS_2 island, which has grown over a G region. (e,f) Larger MoS_2 islands on graphene after an additional cycle of Mo evaporation and H_2S annealing at 1050 K. The image in (f) shows merged islands and atoms inside islands in greater detail. The STM imaging parameters are provided on the images.

preventing the formation of large Mo aggregates. Interestingly, on the graphene areas, the Mo clusters are found to mainly decorate the edges of the graphene. This is in sharp contrast to the dense film of Mo clusters that can be seen inside the buffer layer regions (denoted B in Figure 1b), thereby making the buffer layer easier to distinguish from graphene. The preference for adsorption on the buffer layer is ascribed to its higher reactivity, which has also been confirmed *via* molecular adsorption patterns observed on G/SiC.[40] In a first attempt, the Mo-decorated surface is annealed for 1 h at 1050 K in a H_2S pressure on the order of 1×10^{-5} mbar using a custom-made doser with the nozzle $\approx$1 mm away from the sample surface.[41] This promotes the growth of nanosized MoS_2 islands, which are located predominately in the buffer layer regions in this initial growth stage, as seen in Figure 1c. The STM image in Figure 1d shows an atomically resolved MoS_2 island where the atomic spacing is found to be 3.1 ± 0.3 Å. This island can be seen to already extend onto a single-layer graphene area. Repeating such a growth cycle leads to a gradual increase in the size of islands, as seen in Figure 1e. The island structures and edge shapes deviate substantially from the hexagonal structure and straight edges expected for a free-standing island in thermodynamic equilibrium.[42] Such irregular edges have also been observed for MoS_2 nanoclusters grown on a highly ordered pyrolytic graphite (HOPG) surface, where their occurrence was attributed to defects that act as pinning sites during the growth.[43] The elevated temperatures during growth are likely to increase the mobility of these defects such that they migrate to the edges of the islands and force them to assume an irregular shape. Furthermore, due to the relatively weak interaction between MoS_2 and our graphene substrates, many rotational variants of the MoS_2 islands nucleate. Due to the irregularly shaped edges, it is difficult for these differently rotated islands to coalesce, as evidenced in Figure 1f, where the edges of neighboring islands are seen to line up but not merge seamlessly and, instead, form noticeable domain boundaries. Bright, rounded features are observed on top and around the edges of the MoS_2 islands, which are excess nonsulfurized Mo or partly sulfurized amorphous MoS_2. Their adsorption is presumably facilitated by the higher reactivity at the edges and defect sites in the MoS_2 or in the underlying substrate.

Continuation of the cycled growth leads to extended SL MoS_2 areas as seen for a sample with a coverage of 0.55 ML in the STM image in Figure 2a. In contrast to the MoS_2 nanoislands in Figure 1c, which were mainly localized in the buffer layer areas, the SL MoS_2 is observed to spread across the graphene areas. Since bare buffer layer regions are scarce compared to bare graphene areas, the higher coverage of SL MoS_2 ensures that our samples consist predominantly of MoS_2 on graphene. While clear atomically resolved images of the structure inside the basal plane of MoS_2 could be achieved for the nanoislands, we find it harder to obtain atomic resolution inside the layers in Figure 2a, which may be due to electronic effects associated with the underlying substrate. A smaller

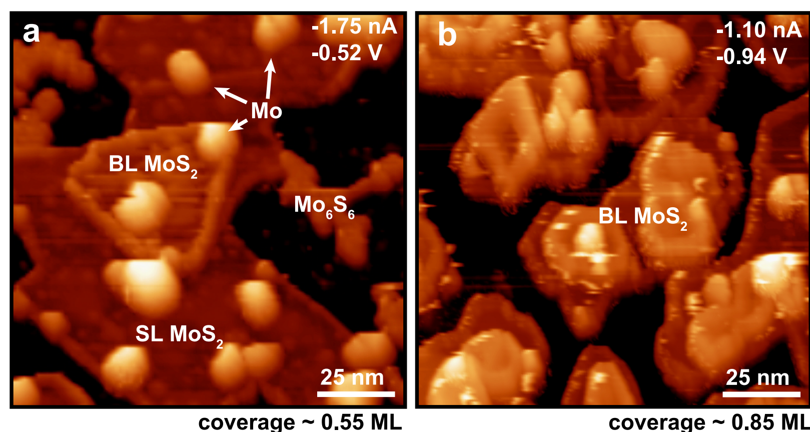

Figure 2. STM images of MoS_2 on G/SiC with a SL MoS_2 coverage of approximately (a) 0.55 ML and (b) 0.85 ML. In (a), bare SL MoS_2 areas coexist with metallic Mo clusters (see arrows) and a BL MoS_2 island. Structures that resemble Mo_6S_6 nanowires are seen on graphene areas. The higher coverage sample in (b) has fewer bare SL MoS_2 areas and a higher number of BL MoS_2 islands. The STM imaging parameters are provided on the images.

BL MoS_2 island appears along with Mo clusters on top of the SL MoS_2. We can distinguish SL and BL MoS_2 by their apparent heights in STM, which we measure to be 8 ± 2 and 17 ± 2 Å, respectively. At the coverage of 0.55 ML, we estimate that 6% is BL MoS_2, which appears to be the limiting case where the presence of BL MoS_2 regions does not influence the laterally averaged electronic structure (on a submillimeter length scale) of the sample measured by ARPES, which we discuss later. Features that lack well-defined structure are observed on bare graphene areas. These may be bundles of Mo_6S_6 nanowires similar to those previously observed on HOPG[44] and Cu(111).[45]

Increasing the coverage to 0.85 ML using additional growth cycles leads to 40% BL MoS_2, which is seen in Figure 2b. The excess metallic Mo clusters act as seeding points for growth of additional MoS_2 layers. Keeping their concentration low, that is, keeping the Mo flux low during evaporation, is the key to favor SL MoS_2 growth. We point out here that in contrast to the growth of $MoSe_2$ films on G/SiC, where co-deposition of atomic Mo and Se using a MBE approach results in $MoSe_2$ after annealing in a single growth cycle,[11,12] the reaction between Mo and S from the H_2S gas source necessitates the cycled approach with very gentle Mo deposition in each cycle. Otherwise, we found that metallic Mo assembles in large clusters, which were either difficult to sulfurize within the limits of the experimental setup or seeds on already nucleated MoS_2 islands leading to multilayer MoS_2.

The valence bands (VBs) of the SL and BL MoS_2–graphene heterostructures are measured by means of ARPES using 70 eV photons, as shown in Figure 3. We directly measure the dominant orientation of the hexagonal Brillouin zone (BZ) of MoS_2 from ARPES data and find it to be rotated 30° with respect to the graphene BZ (see insets in Figure 3). Note, however, that many other orientations are also present. This is a consequence of the weak van der Waals interaction between MoS_2 and the underlying substrate. A cut along the $\bar{K}-\bar{\Gamma}-\bar{K}'$ direction of MoS_2 is presented in Figure 3a. Immediately striking are the intense VB maxima around $\bar{\Gamma}$ and $\bar{K}'$ and the overall remarkable agreement between the experimental dispersion and the calculated band structure for free-standing MoS_2 (dashed white lines).[46] Our data completely reproduce the prediction of the global VB maximum at $\bar{K}$ ($\bar{K}'$) being displaced 0.1 eV toward lower binding energies than the local VB maximum at $\bar{\Gamma}$. Since the conduction band minimum is also located at $\bar{K}$ ($\bar{K}'$),[46] this position of the VB global maximum is consistent with the expectation that SL MoS_2 is a direct gap semiconductor. We are not able to resolve the two spin split bands toward $\bar{K}$ ($\bar{K}'$), which we attribute to the fact that our measurement averages laterally over different rotational variants of MoS_2, thereby broadening the VB features. There are no apparent signatures in the electronic structure from the MoS_2 on buffer layer regions, which is expected because MoS_2/G/SiC areas dominate in our samples, as seen in STM. The clear dispersion of the Dirac states around the $\bar{K}$-points of graphene in Figure 3b,d ensures that there is SL graphene under MoS_2, as the buffer layer does not exhibit the linear Dirac bands.[35] In the $\bar{M}-\bar{\Gamma}-\bar{M}$ direction of MoS_2 shown in Figure 3b, we find a similarly good agreement with the theoretical dispersion. It is noticeable that the bands are extinguished at increasingly negative $k_{\parallel}$ but enhanced toward increasingly positive $k_{\parallel}$. This asymmetric behavior of the photoemission intensity between the lower and upper halves of the BZ is purely an effect of the angular dependence of the MoS_2 photoemission matrix elements. These influence the measured intensity due to the varying angle of incidence between the incoming electric field and the Mo 4*d* and S 3*p* orbitals that make up the VB states.[47]

The main difference in the dispersion for the BL MoS_2 sample shown in Figure 3c,d is the shift of the VB

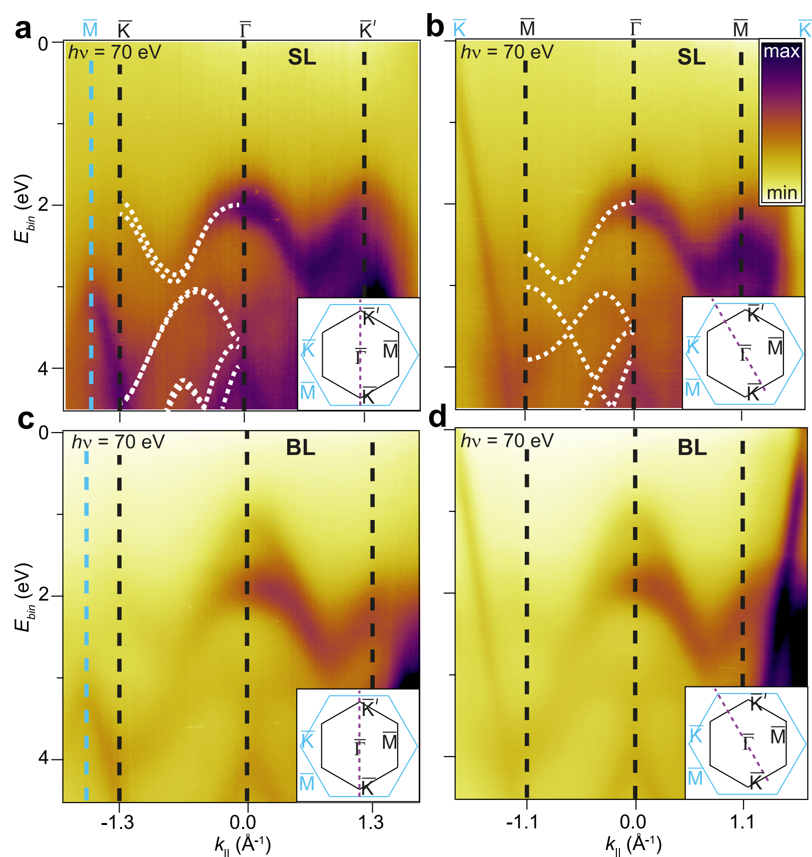

Figure 3. Electronic structure measured by ARPES at a photon energy of 70 eV for (a,b) SL MoS_2 and (c,d) BL MoS_2. The data in (a,c) are cuts along the $\bar{K}-\bar{\Gamma}-\bar{K}'$ direction of the MoS_2 Brillouin zone, while (b,d) present cuts along $\bar{M}-\bar{\Gamma}-\bar{M}$. The MoS_2 (black) and graphene (blue) hexagonal BZs and cut directions are shown in the insets. The dashed white lines in (a,b) correspond to the calculated electronic bands for free-standing SL MoS_2, which have been obtained from ref 46.

global maximum to $\bar{\Gamma}$, which is caused by the appearance of an additional band. This is reminiscent of the situation in the bulk material, which is an indirect gap semiconductor in contrast to the SL case. The overall intensity of the features in the BL sample appears higher than that for the SL sample, which can be understood basically from the higher coverage. We note that the data in Figure 3a,b and c,d were obtained for the exact same samples, as shown in Figure 2a,b, respectively. We have used the ARPES measurements to follow the appearance of the second band at $\bar{\Gamma}$ to determine the critical coverage of 0.55 ML, above which the BL features start to emerge.

Compared to microARPES measurements of exfoliated MoS_2 flakes on a thin SiO_2 substrate, we do not observe a substrate-induced compression of the overall VB bandwidth.[48] Additionally, high-resolution ARPES data from epitaxial SL MoS_2 on Au(111) showed strong hybridization effects between the Au bulk states and the local VB maximum at $\bar{\Gamma}$.[49] The lack of such effects on the G/SiC template applied here shows that the Mo 4d and S 3p atomic orbitals are much less affected by the underlying π-electron system in graphene. This is further substantiated by the lack of hybridization between the Dirac states of graphene and the MoS_2 VBs in Figure 3a–d. Indeed, the observation that the intrinsic band structure of MoS_2 is not as strongly perturbed on G/SiC as on a metal surface is consistent with recent studies of other TMDC–graphene heterostructures on semiconducting substrates.[13,50,51] In general, the electronic decoupling between the individual 2D materials is an important property for the design of heterostructure devices as the intrinsic electronic properties of the separate 2D systems can be expected to be retained in the heterostructure stack.

The actual 2D character of the electronic states is essential for the vast majority of the electronic properties of SL MoS_2,[6] which has prompted us to study these states in further detail by following their dispersion with photon energy, as shown in Figure 4. We focus on the states around $\bar{\Gamma}$, as shown for SL MoS_2 in Figure 4a, because these exhibit the most dramatic change of shape between SL and BL samples. Constant momentum cuts taken in the BZ center show three bands of constant intensity throughout low (18–30 eV) and high photon energy (45–70 eV) ranges for SL MoS_2 in Figure 4b. The local VB maximum is located at a binding energy of 1.9 eV. In the BL case, the additional fourth band has its maximum at a binding energy of 1.3 eV, as seen in Figure 4c. The complete lack of dispersion with photon energy of all the bands in the measured binding energy range indicates that these

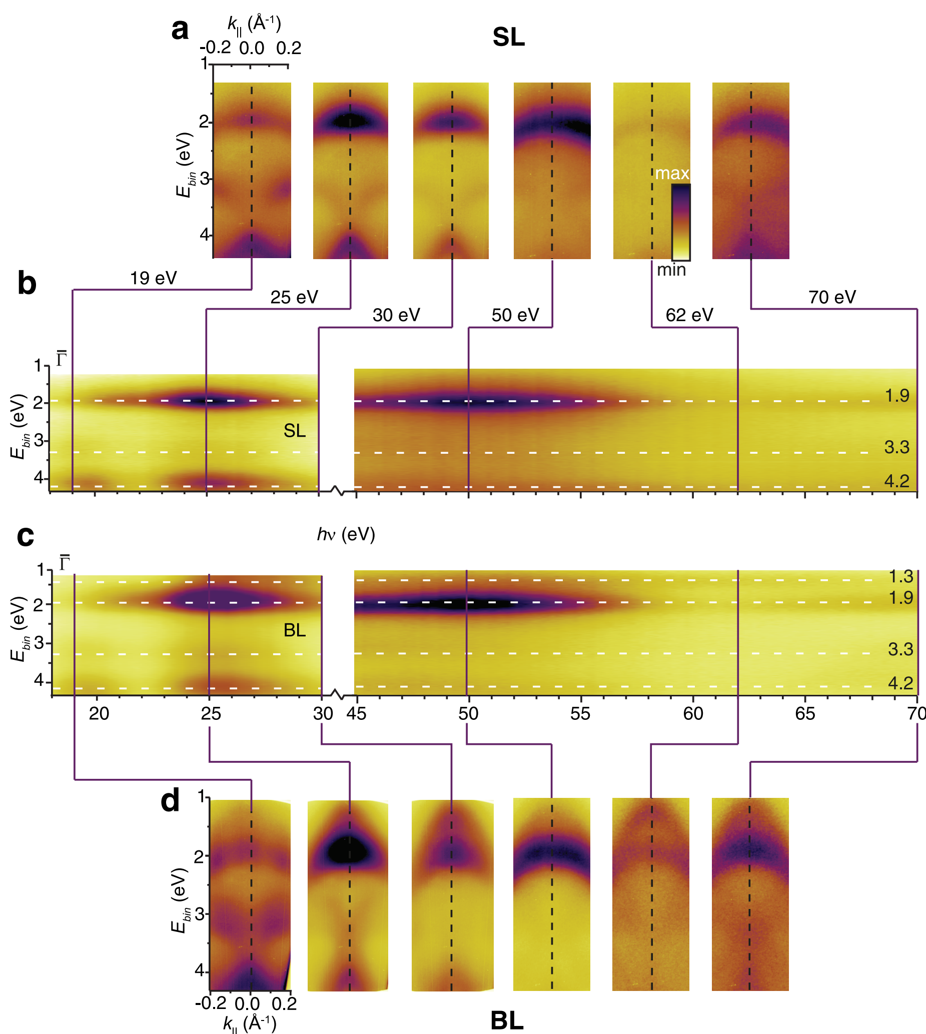

Figure 4. Photon-energy-dependent ARPES measurements, showing the dispersion and intensity variation of the electronic states around $\bar{\Gamma}$ for (a,b) SL MoS_2 and (c,d) BL MoS_2. In (a,d), snapshots of the $k_{||}$-dependent dispersion around $\bar{\Gamma}$ are given at selected photon energies for SL MoS_2 and BL MoS_2, respectively. In (b,c), the photon energy dependence of the photoemission intensity of the states at $\bar{\Gamma}$ is shown for SL MoS_2 and BL MoS_2, respectively. Dashed white lines in (b,c) mark nondispersive states at the energies given to the right in electronvolts.

electronic states belong to the MoS_2 and that these states can indeed be considered genuinely two-dimensional in our heterostructure samples. Strong oscillations in the relative intensities of the bands are detected with pronounced maxima in intensity of the main VB at a binding energy of 1.9 eV for photon energies of 25, 50, and 70 eV. This behavior is analogous to the layer-dependent band structure changes observed for multilayer graphene, where the intensity resonances for the bulk case emerge as the number of layers is increased.[52] Here, this bulk character of the bands is already becoming evident with the addition of the second MoS_2 layer. The differences in appearance of all the studied VBs at specific photon energies are illustrated for SL MoS_2 in Figure 4a and BL MoS_2 in Figure 4d. The cuts have been taken in a direction of the BZ around $\bar{\Gamma}$, where the intensity is symmetric. In the lower photon energy range in Figure 4a,d, these cuts show the bands at higher binding energies with stronger intensities than in the cuts extracted from the higher photon energy range or in Figure 3. We note that in the SL case these bands are again perfectly consistent with the calculation for free-standing SL MoS_2,[46] while in the BL case, subtle differences in the dispersion can be seen. The BL character around $\bar{\Gamma}$ is unmistakable at a photon energy of 62 eV, where the two topmost bands are equally intense. We notice that at photon energies of 19 and 50 eV the topmost BL band is much harder to detect. This deceiving behavior of the photoemission intensity with photon energy is essential to take into account when characterizing the layer-dependent electronic structure of MoS_2. Here, we have provided a scheme to clearly distinguish the electronic structures of SL and BL MoS_2 on graphene.

CONCLUSIONS

A new method has been demonstrated for the *in situ* preparation of SL and BL MoS_2–graphene

heterostructures on a semiconducting silicon carbide substrate, which behave electronically like free-standing MoS_2. The MoS_2 layers were grown by a cycled approach, where the initial evaporated Mo layer seeded on the buffer layer of SiC. Annealing in H_2S led to the nucleation of MoS_2 nanoislands, and an increasing number of growth cycles provided SL MoS_2 with a coverage of 0.55 ML. The electronic structure of this SL MoS_2−graphene heterostructure showed a valence band maximum at the $\bar{K}$ ($\bar{K}'$) point, consistent with this material being a direct gap semiconductor. The overall band structure was found to closely resemble the one expected for free-standing MoS_2 and to be relatively unaffected by the underlying graphene. BL MoS_2 at a coverage of 0.85 ML exhibited a second band around $\bar{\Gamma}$ among the topmost valence band states, which placed the valence band maximum at $\bar{\Gamma}$, suggesting a more bulk-like character. Both SL and BL MoS_2−graphene samples were found to be characterized by electronic states of purely two-dimensional character. We believe that our samples are straightforward to implement in a device scheme, and that they are suitable for optical measurements due to the underlying SiC. This will enable a further exploration of the physics associated with the electrons occupying the $\bar{K}$ and $\bar{K}'$ valleys of the materials. Such experiments may also reveal the properties of the MoS_2−graphene interface, probing the charge transfer dynamics between the different 2D materials. This is important for realizing devices with MoS_2 as the optically active material and graphene as the electrode material. These 2D heterosturctures offer design flexibility and the possibility to combine the remarkable properties of the constituent layers to create new materials. Finally, we believe that our recipe for epitaxially growing a sulfur-based TMDC on graphene will serve as an inspiration to further expand the growing library of two-dimensional materials available for *in situ* characterization and thereby unveil new physics at the single-layer limit.

MATERIALS AND METHODS

Epitaxial Graphene Growth on SiC. A 6H-SiC 2 in. wafer was purchased commercially (TanKeBlue Semiconductor Co. Ltd., n-type doping, 0.02−0.10 $\Omega \cdot$cm) and diced into 4 mm × 7 mm sized pieces to fit our sample holders. The samples were given an initial clean in an isopropyl alcohol ultrasonic bath. The thermally induced growth of epitaxial graphene on the Si-terminated (0001) face of the 6H-SiC substrate was carried out in a dedicated graphene growth chamber with a base pressure of 5×10^{-10} mbar. The samples were degassed *via* direct current heating at a temperature of 825 K for several hours under UHV conditions and subsequently annealed to 1175 K in a mild Si flux for approximately 1 h to remove surface oxides. Following this step, the samples were incrementally flashed to temperatures between 1425 and 1475 K until a clear graphene low energy electron diffraction pattern (not shown) appeared.[35]

Detailed Growth Procedure for MoS_2 on G/SiC. Prior to growing SL MoS_2, the G/SiC substrates were given an anneal to at least 550 K to remove any accumulated adsorbates. Then Mo was deposited from an electron beam evaporator (Oxford Instruments) onto a G/SiC substrate held at room temperature, and from STM measurements, it was determined that the Mo mainly adsorbed on the buffer layer regions of the substrate. Mo deposition was carried out in a low-pressure H_2S atmosphere of $\approx 1 \times 10^{-5}$ mbar. The sample was subsequently annealed to 1050 K for approximately 1 h in the sulfur-rich environment in order to yield irregularly shaped nanometer-sized SL MoS_2 islands. Repeated cycling of this process led to larger-sized SL MoS_2 islands until a coverage of 0.55 ML was reached. Beyond this point, the formation of BL MoS_2 islands began to dominate the growth process. Each step of the synthesis was monitored by STM performed at room temperature under UHV conditions using a home-built Aarhus STM. Tips were etched from W wire. Instrumental artifacts (*i.e.*, piezo creep) were minimized by calibrating STM images using the free WSxM software to reflect the known lattice constant for graphene.[53] Bias voltages stated in the paper refer to the voltage applied to the sample.

ARPES Measurements. The ARPES measurements were carried out at the SGM-3 beamline of the synchrotron radiation source ASTRID2 under UHV conditions with a base pressure in the 10^{-10} mbar range and with the sample temperature kept at 70 K. The photon energy was 70 eV, and the total energy and *k* resolution amounted to 25 meV and 0.02 Å^{-1}, respectively. The photon energy range used to demonstrate the dispersion and intensity variation of the electronic states at $\bar{\Gamma}$ was 18 to 70 eV.

Conflict of Interest: The authors declare no competing financial interest.

Acknowledgment. We gratefully acknowledge funding from the VILLUM foundation, the Lundbeck foundation, the Danish Council for Independent Research, the Danish Strategic Research Council (CAT-C), and Haldor Topsøe A/S. Ph.H. and S.U. acknowledge financial support from the Danish Council for Independent Research, Natural Sciences, under the Sapere Aude program (Grant Nos. DFF-4002-00029 and DFF-4090-00125).

REFERENCES AND NOTES

1. Geim, A.; Grigorieva, I. van der Waals Heterostructures. *Nature* **2013**, *499*, 419–425.
2. Castro Neto, A. H.; Guinea, F.; Peres, N. M. R.; Novoselov, K. S.; Geim, A. K. The Electronic Properties of Graphene. *Rev. Mod. Phys.* **2009**, *81*, 109.
3. Splendiani, A.; Sun, L.; Zhang, Y.; Li, T.; Kim, J.; Chim, C.-Y.; Galli, G.; Wang, F. Emerging Photoluminescence in Monolayer MoS_2. *Nano Lett.* **2010**, *10*, 1271–1275.
4. Ramasubramaniam, A. Large Excitonic Effects in Monolayers of Molybdenum and Tungsten Dichalcogenides. *Phys. Rev. B* **2012**, *86*, 115409.
5. Mak, K.; Lee, C.; Hone, J.; Shan, J.; Heinz, T. Atomically Thin MoS_2: A New Direct-Gap Semiconductor. *Phys. Rev. Lett.* **2010**, *105*, 136805.
6. Wang, Q.; Kourosh, K.; Kis, A.; Coleman, J.; Strano, M. Electronics and Optoelectronics of Two-Dimensional Transition Metal Dichalcogenides. *Nat. Nanotechnol.* **2012**, *7*, 699–712.
7. Xiao, D.; Liu, G.; Feng, W.; Xu, X.; Yao, W. Coupled Spin and Valley Physics in Monolayers of MoS_2 and Other Group-VI Dichalcogenides. *Phys. Rev. Lett.* **2012**, *108*, 196802.
8. Mak, K.; He, K.; Shan, J.; Heinz, T. Control of Valley Polarization in Monolayer MoS_2 by Optical Helicity. *Nat. Nanotechnol.* **2012**, *7*, 494–498.
9. Zeng, H.; Dai, J.; Yao, W.; Xiao, D.; Cui, X. Valley Polarization in MoS_2 Monolayers by Optical Pumping. *Nat. Nanotechnol.* **2012**, *7*, 490–493.

10. Jones, A.; Yu, H.; Ghimire, N.; Wu, S.; Aivazian, G.; Ross, J.; Zhao, B.; Yan, J.; Mandrus, D.; Xiao, D.; et al. Optical Generation of Excitonic Valley Coherence in Monolayer WSe_2. *Nat. Nanotechnol.* **2013**, *8*, 634–638.
11. Zhang, Y.; Chang, T.; Zhou, B.; Cui, Y.; Yan, H.; Liu, Z.; Schmitt, F.; Lee, J.; Moore, R.; Chen, Y.; et al. Direct Observation of the Transition from Indirect to Direct Bandgap in Atomically Thin Epitaxial $MoSe_2$. *Nat. Nanotechnol.* **2014**, *9*, 111–115.
12. Ugeda, M. M.; Bradley, A. J.; Shi, S.-F.; da Jornade, F. H.; Zhang, Y.; Qiu, D. Y.; Ruan, W.; Mo, S.-K.; Hussain, Z.; Shen, Z.-X.; et al. Giant Bandgap Renormalization and Excitonic Effects in a Monolayer Transition Metal Dichalcogenide Semiconductor. *Nat. Mater.* **2014**, *13*, 1091–1095.
13. Lin, Y.; Lu, N.; Nestor, P.; Li, J.; Lin, Z.; Peng, X.; Lee, C.; Sun, C.; Calderin, L.; Browning, P.; et al. Direct Synthesis of van der Waals Solids. *ACS Nano* **2014**, *8*, 3715–3723.
14. Lin, Y.; Chang, C. S.; Ghosh, R.; Li, J.; Zhu, H.; Addou, R.; Diaconescu, B.; Ohta, T.; Peng, X.; Lu, N.; et al. Atomically Thin Heterostructures Based on Single-Layer Tungsten Diselenide and Graphene. *Nano Lett.* **2014**, *14*, 6936–6941.
15. Britnell, L.; Gorbachev, R.; Jalil, R.; Belle, B.; Schedin, F.; Mishchenko, A.; Georgiou, T.; Katsnelson, M.; Eaves, L.; Morozov, S. Field-Effect Tunneling Transistor Based on Vertical Graphene Heterostructures. *Science* **2012**, *335*, 947–950.
16. Britnell, L.; Ribeiro, R. M.; Eckmann, A.; Jalil, R.; Belle, B. D.; Mishchenko, A.; Kim, Y.-J.; Gorbachev, R. V.; Georgiou, T.; Morozov, S. V.; et al. Strong Light−Matter Interactions in Heterostructures of Atomically Thin Films. *Science* **2013**, *340*, 1311–1314.
17. Georgiou, T.; Jalil, R.; Belle, B.; Britnell, L.; Gorbachev, R.; Morozov, S.; Kim, Y.; Gholinia, A.; Haigh, S.; Makarovsky, O.; et al. Vertical Field-Effect Transistor Based on Graphene−WS_2 Heterostructures for Flexible and Transparent Electronics. *Nat. Nanotechnol.* **2013**, *8*, 100–103.
18. Roy, K.; Padmanabhan, M.; Goswami, S.; Sai, T. P.; Ramalingam, G.; Raghavan, S.; Ghosh, A. Graphene−MoS_2 Hybrid Structures for Multifunctional Photoresponsive Memory Devices. *Nat. Nanotechnol.* **2013**, *8*, 826–830.
19. Bernardi, M.; Palummo, M.; Grossman, J. C. Extraordinary Sunlight Absorption and One Nanometer Thick Photovoltaics Using Two-Dimensional Monolayer Materials. *Nano Lett.* **2013**, *13*, 3664–3670.
20. Hong, X.; Kim, J.; Shi, S.-F.; Zhang, Y.; Jin, C.; Sun, Y.; Tongay, S.; Wu, J.; Zhang, Y.; Wang, F. Ultrafast Charge Transfer in Atomically Thin MoS_2/WS_2 Heterostructures. *Nat. Nanotechnol.* **2014**, *9*, 682–686.
21. Ceballos, F.; Bellus, M. Z.; Chiu, H.-Y.; Zhao, H. Ultrafast Charge Separation and Indirect Exciton Formation in a MoS_2−$MoSe_2$ van der Waals Heterostructure. *ACS Nano* **2014**, *8*, 12717–12724.
22. Yu, Y.; Hu, S.; Su, L.; Huang, L.; Liu, Y.; Jin, Z.; Purezky, A. A.; Geohegan, D. B.; Kim, K. W.; Zhang, Y.; et al. Equally Efficient Interlayer Exciton Relaxation and Improved Absorption in Epitaxial and Nonepitaxial MoS_2/WS_2 Heterostructures. *Nano Lett.* **2015**, *15*, 486–491.
23. Hong, Y. J.; Fukui, T. Controlled van der Waals Heteroepitaxy of InAs Nanowires on Carbon Honeycomb Lattices. *ACS Nano* **2011**, *5*, 7576–7584.
24. Kim, J.; Bayram, C.; Park, H.; Cheng, C.; Dimitrakopoulos, C.; Ott, J. A.; Reuter, K. B.; Bedell, S. W.; Sadana, D. K. Principle of Direct van der Waals Epitaxy of Single-Crystalline Films on Epitaxial Graphene. *Nat. Commun.* **2014**, *5*, 4836.
25. Dang, W.; Peng, H.; Li, H.; Wang, P.; Liu, Z. Epitaxial Heterostructures of Ultrathin Topological Insulator Nanoplate and Graphene. *Nano Lett.* **2010**, *10*, 2870–2876.
26. Shi, Y.; Zhou, W.; Lu, A.; Fang, W.; Lee, Y.; Hsu, A.; Kim, S.; Kim, K.; Yang, H.; Li, L.; et al. van der Waals Epitaxy of MoS_2 Layers Using Graphene as Growth Templates. *Nano Lett.* **2012**, *12*, 2784–2791.
27. Lin, M.; Chang, C.; Wang, C.; Su, C.; Chen, C.; Lee, S.; Lin, S. Toward Epitaxially Grown Two-Dimensional Crystal Hetero-structures: Single and Double MoS_2/Graphene Hetero-structures by Chemical Vapor Depositions. *Appl. Phys. Lett.* **2014**, *105*, 073501.
28. McCreary, K. M.; Hanbicki, A. T.; Robinson, J. T.; Cobas, E.; Culbertson, J. C.; Friedman, A. L.; Jernigan, G. G.; Jonker, B. T. Large-Area Synthesis of Continuous and Uniform MoS_2 Monolayer Films on Graphene. *Adv. Funct. Mater.* **2014**, *24*, 6449–6454.
29. McDonnell, S.; Addou, R.; Buie, C.; Wallace, R. M.; Hinkle, C. L. Defect-Dominated Doping and Contact Resistance in MoS_2. *ACS Nano* **2014**, *8*, 2880–2888.
30. Wu, S.; Huang, C.; Aivazian, G.; Ross, J.; Cobden, D.; Xu, X. Vapor−Solid Growth of High Optical Quality MoS_2 Monolayers with Near-Unity Valley Polarization. *ACS Nano* **2013**, *7*, 2768–2772.
31. Wang, Q.; Ge, S.; Li, X.; Qiu, J.; Ji, Y.; Feng, J.; Sun, D. Valley Carrier Dynamics in Monolayer Molybdenum Disulfide from Helicity-Resolved Ultrafast Pump-Probe Spectroscopy. *ACS Nano* **2013**, *7*, 11087–11093.
32. Wang, H.; Zhang, C.; Rana, F. Ultrafast Dynamics of Defect-Assisted Electron−Hole Recombination in Monolayer MoS_2. *Nano Lett.* **2015**, *15*, 339–345.
33. Sørensen, S. G.; Füchtbauer, H. G.; Tuxen, A. K.; Walton, A. S.; Lauritsen, J. V. Structure and Electronic Properties of In Situ Synthesized Single-Layer MoS_2 on a Gold Surface. *ACS Nano* **2014**, *8*, 6788–6796.
34. Forbeaux, I.; Themlin, J.; Charrier, A.; Thibaudau, F.; Debever, J. Solid-State Graphitization Mechanisms of Silicon Carbide 6H-SiC Polar Faces. *Appl. Surf. Sci.* **2000**, *162*−*163*, 406.
35. Emtsev, K. V.; Speck, F.; Seyller, T.; Ley, L.; Riley, J. D. Interaction, Growth, and Ordering of Epitaxial Graphene on SiC(0001) Surfaces: A Comparative Photoelectron Spectroscopy Study. *Phys. Rev. B* **2008**, *77*, 155303.
36. Brar, V. W.; Zhang, Y.; Yayon, Y.; Ohta, T.; McChesney, J. L.; Bostwick, A.; Rotenberg, E.; Horn, K.; Crommie, M. F. Scanning Tunneling Spectroscopy of Inhomogeneous Electronic Structure in Monolayer and Bilayer Graphene on SiC. *Appl. Phys. Lett.* **2007**, *91*, 122102.
37. Mallet, P.; Varchon, F.; Naud, C.; Magaud, L.; Berger, C.; Veuillen, J. Electron States of Mono- and Bilayer Graphene on SiC Probed by Scanning-Tunneling Microscopy. *Phys. Rev. B* **2007**, *76*, 041403(R).
38. Bostwick, A.; Ohta, T.; Seyller, T.; Horn, K.; Rotenberg, E. Quasiparticle Dynamics in Graphene. *Nat. Phys.* **2007**, *3*, 36–40.
39. Ristein, J.; Mammadov, S.; Seyller, T. Origin of Doping in Quasi-Free-Standing Graphene on Silicon Carbide. *Phys. Rev. Lett.* **2012**, *108*, 246104.
40. Wong, S. L.; Huang, H.; Wang, Y.; Cao, L.; Qi, D.; Santoso, I.; Chen, W.; Wee, A. T. S. Quasi-Free-Standing Epitaxial Graphene on SiC (0001) by Fluorine Intercalation from a Molecular Source. *ACS Nano* **2011**, *5*, 7662–7668.
41. Lauritsen, J. V.; Besenbacher, F. Model Catalyst Surfaces Investigated by Scanning Tunneling Microscopy. *Adv. Catal.* **2006**, *50*, 97–147.
42. Lauritsen, J. V.; Bollinger, M. V.; Lægsgaard, E.; Jacobsen, K. W.; Nørskov, J. K.; Clausen, B. S.; Topsøe, H.; Besenbacher, F. Atomic-Scale Insight into Structure and Morphology Changes of MoS_2 Nanoclusters in Hydrotreating Catalysts. *J. Catal.* **2004**, *221*, 510–522.
43. Kibsgaard, J.; Lauritsen, J. V.; Lægsgaard, E.; Clausen, B. S.; Topsøe, H.; Besenbacher, F. Cluster-Support Interactions and Morphology of MoS_2 Nanoclusters in a Graphite-Supported Hydrotreating Model Catalyst. *J. Am. Chem. Soc.* **2006**, *128*, 13950–13958.
44. Kibsgaard, J.; Tuxen, A.; Levisen, M.; Lægsgaard, E.; Gemming, S.; Seifert, G.; Lauritsen, J. V.; Besenbacher, F. Atomic-Scale Structure of Mo_6S_6 Nanowires. *Nano Lett.* **2008**, *8*, 3928–3931.
45. Le, D.; Sun, D.; Lu, W.; Aminpour, M.; Wang, C.; Ma, Q.; Rahman, T. S.; Bartels, L. Growth of Aligned Mo_6S_6 Nanowires on Cu(111). *Surf. Sci.* **2013**, *611*, 1–4.
46. Zhu, Z. Y.; Cheng, Y. C.; Schwingenschlögl, U. Giant Spin−Orbit-Induced Spin Splitting in Two-Dimensional Transition-Metal Dichalcogenide Semiconductors. *Phys. Rev. B* **2011**, *84*, 153402.
47. Komesu, T.; Le, D.; Ma, Q.; Schwier, E. F.; Kojima, Y.; Zheng, M.; Iwasawa, H.; Shimada, K.; Taniguchi, M.; Bartels, L.; et al.

Symmetry-Resolved Surface Derived Electronic Structure of MoS_2(0001). *J. Phys.: Condens. Matter* **2014**, *26*, 455501.
48. Jin, W.; Yeh, P.; Zaki, N.; Zhang, D.; Sadowski, J. T.; Al-Mahboob, A.; van der Zande, A. M.; Chenet, D. A.; Dadap, J. I.; Herman, I. P.; et al. Direct Measurement of the Thickness-Dependent Electronic Band Structure of MoS_2 Using Angle-Resolved Photoemission Spectroscopy. *Phys. Rev. Lett.* **2013**, *111*, 106801.
49. Miwa, J. A.; Ulstrup, S.; Sørensen, S. G.; Dendzik, M.; Čabo, A. G.; Bianchi, M.; Lauritsen, J. V.; Hofmann, P. Electronic Structure of Epitaxial Single-Layer MoS_2. *Phys. Rev. Lett.* **2015**, *114*, 046802.
50. Shim, G. W.; Yoo, K.; Seo, S.-B.; Shin, J.; Jung, D. Y.; Kang, I.-S.; Ahn, C. W.; Cho, B. J.; Choi, S.-Y. Large-Area Single-Layer $MoSe_2$ and Its van der Waals Heterostructures. *ACS Nano* **2014**, *8*, 6655–6662.
51. He, J.; Kumar, N.; Bellus, M. Z.; Chiu, H.-Y.; He, D.; Wang, Y.; Zhao, H. Electron Transfer and Coupling in Graphene–Tungsten Disulfide van der Waals Heterostructures. *Nat. Commun.* **2014**, *5*, 5622.
52. Ohta, T.; Bostwick, A.; McChesney, J. L.; Seyller, T.; Horn, K.; Rotenberg, E. Interlayer Interaction and Electronic Screening in Multilayer Graphene Investigated with Angle-Resolved Photoemission Spectroscopy. *Phys. Rev. Lett.* **2007**, *98*, 206802.
53. Horcas, I.; Fernández, R.; Gómez-Rodríguez, J. M.; Colchero, J.; Gómez-Herrero, J.; Baro, A. M. WSXM: A Software for Scanning Probe Microscopy and a Tool for Nanotechnology. *Rev. Sci. Instrum.* **2007**, *78*, 013705.